ISSN 1063-7834, Physics of the Solid State, 2014, Vol. 56, No. 3, pp. 599–605. © Pleiades Publishing, Ltd., 2014.
Original Russian Text © Yu.V. Gerasimova, A.S. Oreshonkov, A.A. Ivanenko, M.S. Molokeev, L.I. Isaenko, I.N. Flerov, E.V. Bogdanov, M.V. Gorev, A.V. Kartashev, A.S. Krylov, 2014, published in Fizika Tverdogo Tela, 2014, Vol. 56, No. 3, pp. 577–582.

LATTICE DYNAMICS

Structural, Spectroscopic, and Thermophysical Investigations of the Oxyfluorides $CsZnMoO_3F_3$ and $CsMnMoO_3F_3$ with the Pyrochlore Structure

Yu. V. Gerasimova[a, *], A. S. Oreshonkov[a], A. A. Ivanenko[a], M. S. Molokeev[a], L. I. Isaenko[b], I. N. Flerov[a, c], E. V. Bogdanov[a], M. V. Gorev[a, c], A. V. Kartashev[a], and A. S. Krylov[a]

[a] *Kirensky Institute of Physics, Siberian Branch of the Russian Academy of Sciences, Akademgorodok 50–38, Krasnoyarsk, 660036 Russia*

** e-mail: jul@iph.krasn.ru*

[b] *Sobolev Institute of Geology and Mineralogy, Siberian Branch of the Russian Academy of Sciences, pr. Akademika Koptyuga 3, Novosibirsk, 630090 Russia*

[c] *Institute of Engineering Physics and Radio Electronics, Siberian Federal University, ul. Kirenskogo 28, Krasnoyarsk, 660074 Russia*

Received August 2, 2013

Abstract—The structure, infrared and Raman spectra, heat capacity, and thermal expansion have been investigated. It has been shown that, down to liquid-helium temperatures, the cubic pyrochlore structure of the $CsMnMoO_3F_3$ and $CsZnMoO_3F_3$ oxyfluorides remains stable. The influence of cation substitution on individual features of the properties of the oxyfluorides has been analyzed.

DOI: 10.1134/S1063783414030135

1. INTRODUCTION

Oxyfluorides containing six-coordinated quasi-octahedral ionic groups $(MeF_2O_{6-x})^{3-}$ in the crystal lattice form a wide variety of compounds that are of considerable interest from both the fundamental and applied points of view, in particular, owing to the possibility of varying the composition of fluorine–oxygen (F/O) ligands, which leads to significant changes in the structure and physical properties [1–5]. Compounds with $(MeO_3F_3)^{3-}$ anions often crystallize in a cubic structure despite the quasi-octahedral local symmetry of the anions. Because of the difference in charges of the fluorine and oxygen ions and the displacement of the central atom toward the direction of the oxygen atoms, the fluorine–oxygen quasi-octahedra have a significant dipole moment. The absence of macroscopic polarization is caused by at least two factors associated with the disordering of the F/O ligands or relative orientations of the adjacent octahedra. This situation occurs, for example, in two families of crystals with the general formulas $A_2^+(A^+)'MeO_3F_3$ and $A^+A^{2+}MeO_3F_3$ (where Me is a hexavalent cation). In the first case, for the ratio of ionic radii $R_A > R_{A'}$ or when $A = A'$, the compounds have a crystal structure of the elpasolite–cryolite type (space group $Fm\bar{3}m$, $Z = 4$) [6]. The compounds with a combination of cations A^+A^{2+} have a defect pyrochlore structure (space group $Fd\bar{3}m$, $Z = 8$) [7, 8].

Intensive investigations of elpasolite-like oxyfluorides $A_2^+(A^+)'MeO_3F_3$ (A^+ (A^+)' = Na, K, NH_4, Rb, Cs; Me = Mo, W) demonstrated that, upon cooling, many of them undergo structural phase transitions associated with partial or complete ordering of the fluorine and oxygen ligands disordered in the cubic $Fm\bar{3}m$ phase. As a result, crystals of this family exhibit interesting properties, such as ferroelectricity and ferroelasticity [9–12]. Moreover, it was found that some of these compounds [13, 14] can be considered as classical multiferroics due to the dual nature of phase transitions from the cubic phase, which are caused by the simultaneous occurrence of spontaneous polarization and ferroelastic twinning. The compounds with molybdenum and tungsten, which undergo transformations of the order–disorder type with rather large values of the entropy change, are characterized by a significant difference in susceptibility to hydrostatic pressure. Owing to the large values of the pressure coefficient dT/dp, some of the compounds with $(MoO_3F_3)^{3-}$ anions have significant values of the intensive and extensive barocaloric effects, which are comparable to the values of the electrocaloric and magnetocaloric effects in materials considered as promising solid-state refrigerants [12].

Until now, there is only a rather scarce information about structural characteristics and, especially, physical properties of compounds $A^+A^{2+}MeO_3F_3$ (A^+ = Cs; A^{2+} = Ni, Zn, Mn, Co; Me = Mo, W) [7, 8]. Nonethe-

Table 1. Crystallographic data, data collection, and structure refinement parameters

Space group	$Fd\bar{3}m$
a, Å	10.43818(7)
V, Å^3	1137.30(2)
2θ angle range, deg	5–120
Number of Bragg reflections	58
Number of refined parameters	26
R_B, %	1.735
R_{wp}, %	8.228
R_p, %	6.324
R_{exp}, %	5.670
χ^2	1.451

R_B is the Bragg reliability factor, R_{wp} is the weighted-profile reliability factor, R_p is the profile reliability factor, R_{exp} is the expected reliability factor, and $\chi^2 = R_{wp}/R_{exp}$ is the goodness-of-fit.

Table 2. Atomic coordinates, site occupancies (p), and isotropic thermal parameters (B_{iso}) of the $CsZnMoO_3F_3$ and $CsMnMoO_3F_3$ structures

$CsZnMoO_3F_3$						
Atom	Position	X	Y	Z	p	B_{iso}, Å^2
Cs	8*b*	3/8	3/8	3/8	1.0	4.15(5)
Zn	16*c*	0	0	0	0.5	3.46(5)
Mo	16*c*	0	0	0	0.5	3.46(5)
F	48*f*	1/8	5/8	0.4321(3)	0.5	3.2(1)
O	48*f*	1/8	5/8	0.4321(3)	0.5	3.2(1)
$CsMnMoO_3F_3$						
Atom	Position	X	Y	Z	p	B_{iso}, Å^2
Cs	8*b*	3/8	3/8	3/8	1.0	4.82(4)
Mo	16*c*	0	0	0	0.5	3.72(4)
Mn	16*c*	0	0	0	0.5	3.72(4)
F	48*f*	1/8	5/8	0.4308(3)	0.5	4.6(1)
O	48*f*	1/8	5/8	0.4308(3)	0.5	4.6(1)

less, from the foregoing, it can be assumed that these crystals, which, according to the cubic symmetry, possess a fluorine–oxygen disorder, can exhibit properties similar to those of elpasolite-type crystals. On the other hand, magnetic compounds containing Fe and Mn are of particular importance from the viewpoint of their potential practical use [14–16]. Therefore, the investigation of oxyfluorides based on the $(MeO_3F_3)^{3-}$ anionic groups containing magnetic cations is promising from the viewpoint of the search for new ferroics and multiferroics. It should be noted that some of the manganese-containing oxyfluorides with a partial replacement of O^{2-} by F^- were recently synthesized by the fluorination [17–19]. As regards the crystals with $(MeO_3F_3)^{3-}$ anionic groups, only the $CsMnMoO_3F_3$ compound with space group $Fd\bar{3}m$ was reported previously, but without a detailed description of the structural and, especially, physical properties [6]. Recently, the structural characteristics and the magnetic and electronic properties of the $CsMnMoO_3F_3$ oxyfluoride were investigated in [20].

With the aim of studying the stability of the pyrochlore crystal lattice in oxyfluorides, in this work we investigated the structure, infrared (IR) and Raman spectra, and thermophysical properties of the $CsZnMoO_3F_3$ and $CsMnMoO_3F_3$ compounds.

2. SYNTHESIS

Crystals of the $CsMnMoO_3F_3$ and $CsZnMoO_3F_3$ compounds were grown by the spontaneous crystallization from flux. The compounds were synthesized from the anhydrous fluorides MnF_2, ZnF_2, and CsF, as well as from MoO_3 calcined at a temperature of 600°C, which were taken in stoichiometric ratios: MnF_2 (ZnF_2) + CsF + MoO_3 = $CsMn(Zn)MoO_3F_3$. As a result, the samples were obtained in the form of small intergrowths of cubic crystals.

3. STRUCTURE AND ELECTRON DENSITY

The structure of the $CsMnMoO_3F_3$ oxyfluoride was refined earlier in [20]. In the present work, it was used to investigate the influence of changes in the chemical pressure due to the substitution for the divalent cation on the structural parameters.

The X-ray diffraction analysis of the polycrystalline sample of $CsZnMoO_3F_3$ was performed at room temperature on a D8-ADVANCE diffractometer (CuK_α radiation, θ–2θ scan mode) using a VANTEC linear detector. The X-ray diffraction pattern of the $CsZnMoO_3F_3$ sample was used to refine the structure by the Rietveld method. The initial parameters of the crystallographic cell were the data taken from [7]. The refinement of the parameters was carried out during fitting of the reflection profiles with the TOPAS 4.2 program [21]. Table 1 presents the selected crystal data and the parameters of data collection and structure refinement.

The analysis of the extinctions of reflections confirmed that the crystal structure of the $CsZnMoO_3F_3$ compound actually has cubic symmetry with space group $Fd\bar{3}m$. The search and refinement of the structure were performed in the same way as for the $CsMnMoO_3F_3$ compound [20]. The atomic coordinates, site occupancies, and isotropic thermal parameters are presented in Table 2, together with the data for the manganese oxyfluoride.

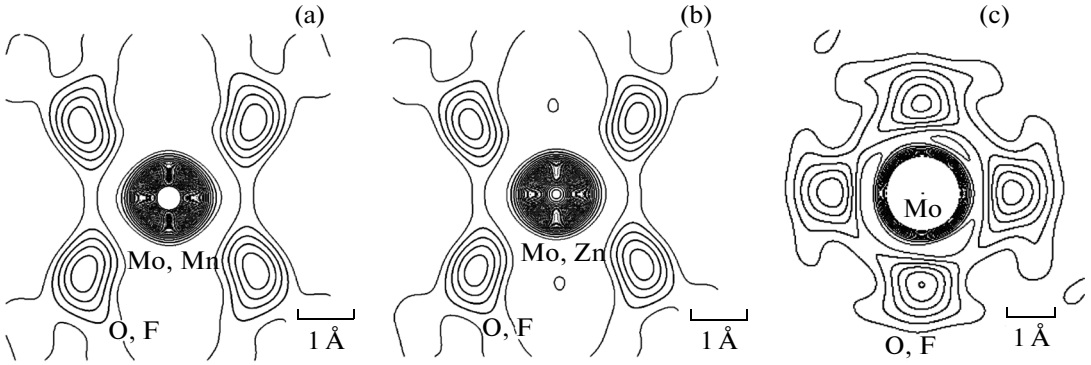

Fig. 1. Electron density maps (with a step of 0.1 e/Å^3) for the octahedra (a) (Mn)MoO_3F_3, (b) (Zn)MoO_3F_3, and (c) $(NH_4)MoO_3F_3$ in the $(NH_4)_3MoO_3F_3$ elpasolite [11].

A comparison of the $CsZnMoO_3F_3$ and $CsMnMoO_3F_3$ structures did not reveal significant differences. In accordance with the ratio of ionic radii of Zn (0.74 Å) and Mn (0.83 Å), the decrease in the cubic unit cell parameter by 0.15 Å in $CsZnMoO_3F_3$ as well as the bond lengths d(Zn(Mo)–O) = 1.977 Å and d(Mn(Mo)–O) = 2.011 (2) Å are quite reasonable. The thermal parameters of heavy atoms in these structures are also close to each other. Only the thermal parameter of the F(O) atoms in the $CsMnMoO_3F_3$ compound is almost one and a half times larger than that in the $CsZnMoO_3F_3$ compound. At the same time, the analysis of the electron density maps obtained by the section of quasi-octahedra through the central atoms and O(F) ligands did not reveal substantial differences in the shapes of the electron density distributions (Fig. 1). This indicates the absence of a pronounced anharmonicity of atomic vibrations in the six-coordinated anionic groups, which could lead to a dynamic disordering of the structure. Thus, it can be assumed that the cubic symmetry of the studied oxyfluorides with the pyrochlore structure is associated with positional disordering of the quasi-octahedra with ordered ligands having such a mutual orientation that leads to a compensation of the dipole moments of the adjacent structural units. It is interesting to compare the electron density maps of molybdenum quasi-octahedra of the same composition in cubic structures of pyrochlore and elpasolite (Fig. 1). It can be seen that, in the $(NH_4)_3MoO_3F_3$ compound, which undergoes a phase transition of the order–disorder type [11], vibrations of the ligands are characterized by a more significant anisotropy.

4. INFRARED ABSORPTION AND RAMAN SCATTERING SPECTRA

The IR absorption spectra were recorded on a Bruker VERTEX 80v vacuum Fourier transform infrared (FT-IR) spectrometer using tablets (13 mm in diameter and ~0.55 mm thick) pressed together with potassium bromide in a 1 : 100 ratio. The Raman spectra were measured on a Horiba Jobin Yvon T64000 spectrometer in the backscattering geometry. The spectra were excited by radiation from an Ar^+ laser operating at the wavelength $\lambda = 514.5$ nm. The radiation power at the sample was less than 5 mW.

In the cubic phase, the expansion of the vibrational representation at the center of the Brillouin zone of the compounds has the form

$$\Gamma(Fd\bar{3}m) = 4A_{2u} + 4E_u + 11F_u + 6T_u + 2A_{1g} + 2E_g + 4F_g + 7T_g,$$

$$\Gamma_{\text{Raman}} = 2A_{1g} + 2E_g + 7T_g,$$

$$\Gamma_{\text{IR}} = 11F_u.$$

In order to interpret active modes, we performed a semiempirical calculation of the lattice dynamics of the studied compounds with the LADY software package [22]. It turned out that the simplest "rigid-ion" model is quite applicable to describe the spectra of these compounds. The model describes the interaction of isolated spherical ions with the charge Z_i. The potential function is represented as the sum of the Coulomb potential and the interatomic interaction potential described by the Born–Mayer function [23]. The parameters of the computational model were optimized taking into account the lattice stability conditions. Using the atom–atom interaction potential parameters, we calculated the complete vibrational spectrum of the studied crystal and eigenvectors of the modes active in IR and Raman spectra.

The experimental Raman and IR spectra of the $CsMnMoO_3F_3$ and $CsZnMoO_3F_3$ compounds at room temperature are shown in Figs. 2a and 2b.

In the structure of the studied crystals, the cesium atom is surrounded by twelve vertex-shared quasi-octahedra Mn(Zn)O_3F_3 and MnO_3F_3 [20]. According to the performed calculation, the Raman spectra of the $CsMnMoO_3F_3$ compound exhibit totally symmetric vibrations of the environment of the cesium atoms

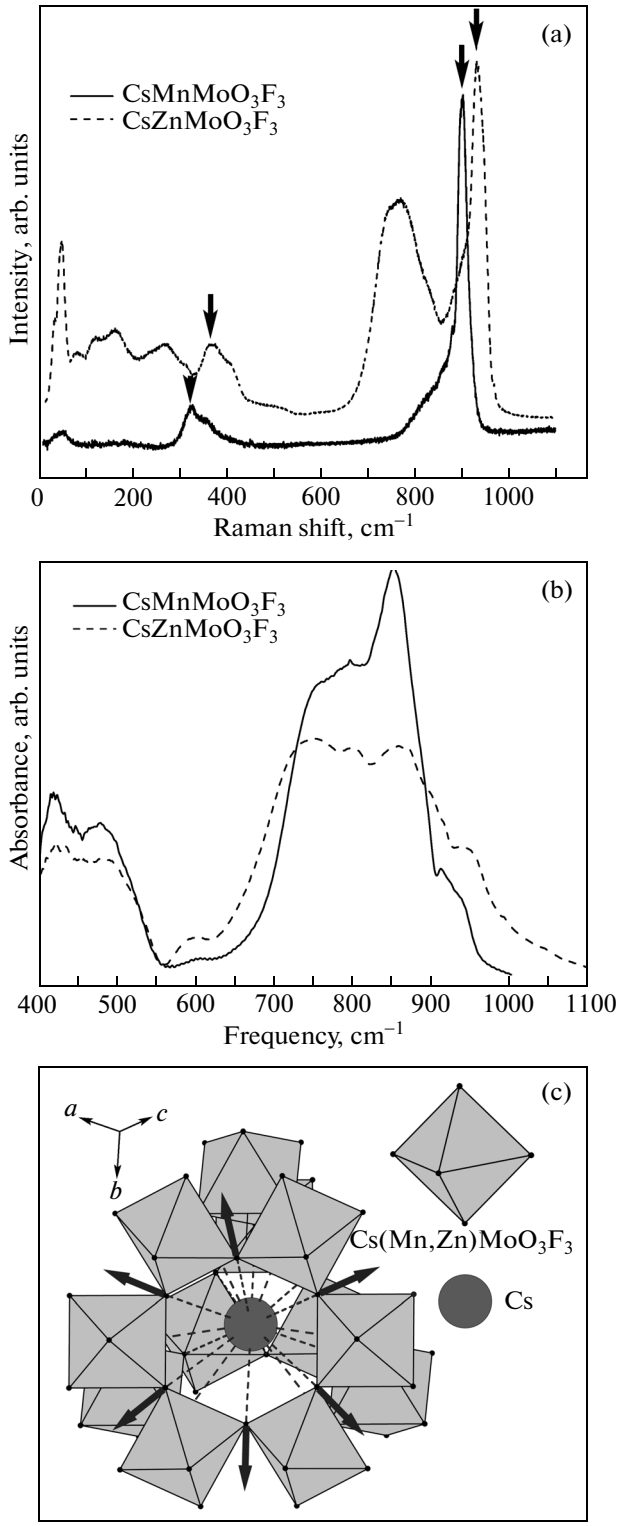

Fig. 2. Experimental (a) Raman and (b) IR spectra of the $CsMnMoO_3F_3$ and $CsZnMoO_3F_3$ compounds at room temperature. (c) Totally symmetric vibrations in the environment of the cesium atoms (shown by arrows in the Raman spectra).

at frequencies of 323 and 900 cm^{-1} (A_{1g}) (Fig. 2c). The spectral line at 323 cm^{-1} predominantly corresponds to vibrations of the fluorine atoms along the Cs–F bond, and the line at 900 cm^{-1}, to vibrations of the oxygen atoms along the Cs–O bond. A similar pattern is observed for the $CsZnMoO_3F_3$ compound: the corresponding vibrations occur at frequencies of 370 and 930 cm^{-1}. The only Raman-active lattice vibrational mode (T_g) is observed at frequencies of 50 and 48 cm^{-1} for the $CsMnMoO_3F_3$ and $CsZnMoO_3F_3$ compounds, respectively, and relates to vibrations of the Cs atoms. The spectral region located between the low-frequency lattice vibrational mode and the totally symmetric vibrational mode of the fluorine atoms corresponds to vibrations of the octahedral groups as a whole. The differences in the distributions of the relative intensities of vibrations in this region for the studied compounds, most likely, are associated with different polarizabilities of the manganese and zinc ions.

The IR spectra of the $CsMnMoO_3F_3$ and $CsZnMoO_3F_3$ compounds can be conventionally separated into two regions: 550–1000 cm^{-1} is the frequency range of polar strains of the octahedral environment of the cesium atoms and 450–550 cm^{-1} is the range of bending vibrations of the $Mn(Zn)O_3F_3$ and MoO_3F_3 octahedral groups. For both compounds, there is an equal number of active vibrations in the frequency range of 550–1000 cm^{-1}, but the intensities of the lines of the corresponding vibrations are different. A possible reason can be differences in the effective charges of the Mn and Zn ions.

It should be noted that the IR and Raman spectra of the manganese and zinc compounds obey the alternative prohibition rule despite the fact that the cubic structure of these crystals is substantially disordered.

The IR spectra of the $CsZn(Mn)MoO_3F_3$ compounds at different temperatures are shown in Fig. 3. The Raman spectra of the $CsMnMoO_3F_3$ compounds at different temperatures are presented in Fig. 4. It can be seen that, down to liquid-helium temperatures, the vibrational spectra do not exhibit noticeable changes that could be attributed to structural phase transitions.

5. HEAT CAPACITY AND THERMAL EXPANSION

The temperature dependence of the isobaric heat capacity $C_p(T)$ in the temperature range of 80–300 K was measured on an adiabatic calorimeter during continuous and discrete heatings. The error in the determination of the heat capacity did not exceed 0.5% over the entire temperature range studied. The calorimetric measurements were performed on pressed samples weighing 80 and 170 mg, which were prepared from ground polycrystalline compounds $CsMnMoO_3F_3$ and $CsZnMoO_3F_3$. A more detailed description of the methodological features of the experiment was given

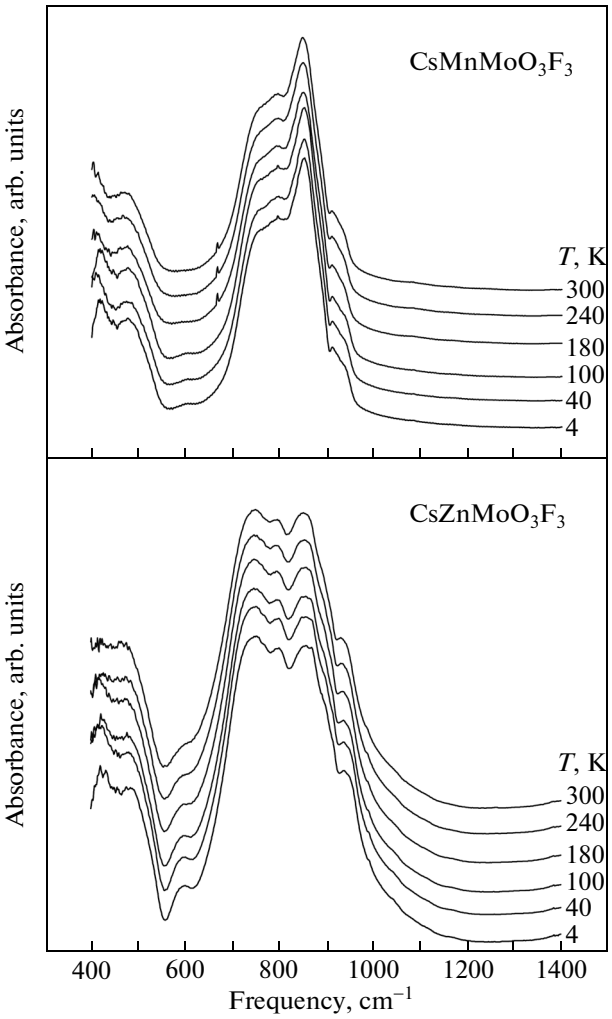

Fig. 3. IR spectra of the $CsMnMoO_3F_3$ and $CsZnMoO_3F_3$ compounds at different temperatures.

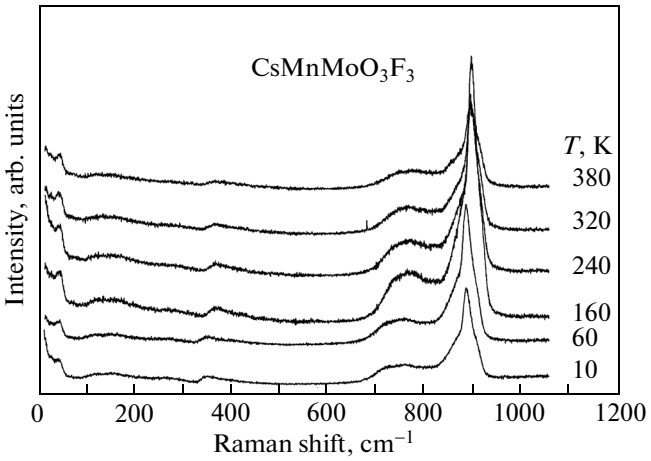

Fig. 4. Raman spectra of the $CsMnMoO_3F_3$ compounds at different temperatures.

in [24]. The temperature dependences of the molar heat capacity for both compounds are shown in Fig. 5a. It is seen from this figure that an anomalous behavior of $C_p(T)$ due to possible phase transformations is not observed at least down to 80 K. As is also seen, the substitution Zn ⟶ Mn leads to an increase in the heat capacity by 6–8% in the temperature range studied.

The temperature dependence of the linear thermal expansion coefficient $\alpha(T)$ was investigated in the temperature range of 100–320 K on a NETZSCH DIL-402C inductive dilatometer in the dynamic mode at heating rates of 2–5 K/min. The measurements were performed in a stream of dry helium. The calibration and correction for thermal expansion of the measuring system were carried out using fused silica reference samples. The dilatometric investigations were performed on samples in the form of tablets prepared by pressing powders. The sizes of the samples along the measurement direction were equal to 8.01 mm for $CsZnMoO_3F_3$ and 4.3 mm for $CsMnMoO_3F_3$).

The results of measurements in the form of the volume thermal expansion coefficient $\beta = 3\alpha$ are presented in Fig. 5b. As in the calorimetric and spectroscopic investigations, no anomalies in the dependences $\beta(T)$ for both compounds were found. It should be noted that primary measurements of the thermal expansion revealed anomalies of $\beta(T)$ at temperatures in the range of 270–290 K (Fig. 5c). However, during repeated thermal cycling, anomaly decreased and disappeared altogether. A possible reason for this phenomenon can be related to the presence of some moisture in the as-pressed samples due to their hygroscopicity. The absence of relevant anomalies on the heat capacity curves is explained by the fact that the calorimetric investigations were performed in a high vacuum.

A noteworthy result is a significant difference between the thermal expansion coefficients of the studied samples. In the temperature region of thermal expansion measurements, the coefficient β varies in the ranges $(55–65) \times 10^{-6}$ K^{-1} for $CsMnMoO_3F_3$ and $(30–40) \times 10^{-6}$ K^{-1} for $CsZnMoO_3F_3$ (Fig. 5b). The thermal expansion is determined by anharmonicity of atomic vibrations in the crystal structure, and the parameter characterizing the degree of anharmonicity of atomic vibrations is the ratio between the squares of the average displacement of the atoms and the unit cell parameter $\delta = \langle x^2 \rangle / a_0^2$ [25]. In turn, there is a direct relationship between $\langle x^2 \rangle$ and the thermal factor $B_{iso} = 8\pi^2 \langle x^2 \rangle$. In structural investigations, we revealed that the thermal parameter of vibrations of the F/O ligands in the manganese oxyfluoride ($B_{iso} = 4.6$ Å^2) is substantially larger than that in the zinc oxyfluoride ($B_{iso} = 3.4$ Å^2). Thus, it can be assumed that this circumstance is responsible for the significant difference

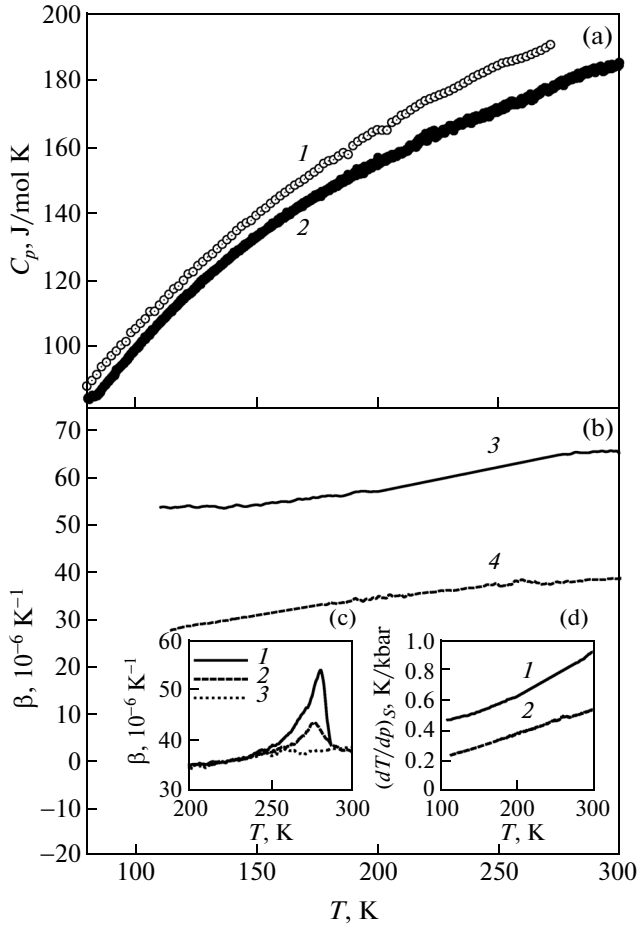

Fig. 5. Temperature dependences of (a) the heat capacity and (b) the volume thermal expansion coefficient for (*1*) $CsMnMoO_3F_3$ and (*2*) $CsZnMoO_3F_3$ compounds. (c) Behavior of β(*T*) during successive heatings *1–3*. (d) Temperature dependences of the barocaloric coefficient for (*1*) $CsMnMoO_3F_3$ and (*2*) $CsZnMoO_3F_3$.

between the volume thermal expansion coefficients of the studied oxyfluorides.

The obtained data on the heat capacity and thermal expansion coefficient allow us to analyze their relation in terms of the standard thermodynamic equation $C_p = Tv(\partial p/\partial T)_S\beta$ and to obtain information on the temperature dependence of the adiabatic temperature coefficient of pressure. Figure 5d presents the inverse derivative $(\partial T/\partial p)_S$ (barocaloric coefficient), which characterizes the change in temperature under pressure at a constant entropy. It can be seen from this figure that, with an increase in the temperature, the barocaloric coefficient $(\partial T/\partial p)_S$ for $CsMnMoO_3F_3$ increases more rapidly. However, even at 300 K, the observed barocaloric effect is small compared with the characteristic values for elpasolite-like oxyfluorides in the phase transition region [12].

6. CONCLUSIONS

The influence of cation substitution on the structural, spectral, and thermophysical properties of the $CsMnMoO_3F_3$ and $CsZnMoO_3F_3$ oxyfluorides with the pyrochlore structure (space group $Fd\bar{3}m$, $Z = 8$) has been investigated. No phase transitions have been found; i.e., the cubic structure of both compounds remains stable down to liquid-helium temperatures.

The performed analysis of the IR and Raman spectra allowed us to assume that the observed difference in relative intensities of the vibrations at frequencies of 550–1000 cm^{-1} in the oxyfluorides can be associated with the differences in effective charges and polarizabilities of the Mn and Zn ions. Despite the disordering in structures of the studied crystals, the spectra obey the alternative prohibition rule.

It has been found that a decrease in the size of the divalent cation leads to a substantial decrease in the thermal parameters B_{iso} of the ligands. However, the character of the electron density distribution of the F/O atoms remains almost unchanged. A significant difference in the values of B_{iso} due to the change in anharmonicity of atomic vibrations was assumed to be responsible for the experimentally established decrease (by a factor of 1.5) in the volume thermal expansion coefficient of $CsZnMoO_3F_3$. Accordingly, the established difference in the barocaloric coefficients $(\partial T/\partial p)_S$ for the studied oxyfluorides also proved to be reasonable.

Returning to the problem of thermal stability of the pyrochlore structure of the studied crystals, attention should be paid to the fact that the study of the cation substitution in the series of elpasolites A_2^+ $(A^+)'WO_3F_3$ ($A^+(A^+)'$ = K, NH_4, Cs) also revealed combinations of monovalent cations stabilizing the cubic phase $Fm\bar{3}m$ down to liquid-helium temperatures [26]. In both cases, as in the pyrochlore structure, the inter-octahedral cavity was occupied by the large cation Cs^+. It is likely that one of the directions in the search for distorted pyrochlore phases can be associated with the synthesis of compounds by means of the substitution Cs ⟶ Rb (NH_4, K) or Mo ⟶ W.

ACKNOWLEDGMENTS

This study was supported by the Russian Foundation for Basic Research (project no. 12-02-31205_mol_a), the Ministry of Education and Science of the Russian Federation within the framework of the Federal Target Program "Scientific and Scientific–Pedagogical Human Resources for the Innovative Russia" (agreement no. 8379), and the Siberian Branch of the Russian Academy of Sciences (Interdisciplinary Integration Project no. 28).

REFERENCES

1. P. A. Maggard, T. S. Nault, C. L. Stern, and K. R. Poeppelmeier, J. Solid State Chem. **175**, 27 (2003).
2. M. R. Marvel, J. Lesage, J. Baek, P. S. Halasyamani, C. L. Stern, and K. R. Poeppelmeier, J. Am. Chem. Soc. **129**, 13963 (2007).
3. J. M. Chamberlain, T. A. Albrecht, J. Lesage, F. Sauvage, C. L. Stern, and K. R. Poeppelmeier, Cryst. Growth Des. **10**, 4868 (2010).
4. A. M. Fry, H. A. Seibel, I. N. Lokuhewa, and P. M. Woodward, J. Am. Chem. Soc. **134**, 2621 (2012).
5. V. V. Atuchin, L. I. Isaenko, V. G. Kesler, Z. S. Lin, M. S. Molokeev, A. P. Yelisseyev, and S. A. Zhurkov, J. Solid Chem. **187**, 159 (2012).
6. G. Pausewang and W. Z. Rüdorff, Z. Anorg. Allg. Chem. **364**, 69 (1969).
7. D. Babel, G. Pausewang, and W. Viebahn, Z. Naturforsch., B: Anorg. Chem., Org. Chem., Biochem., Biophys., Biol. **22**, 1219 (1967).
8. R. Matters, V. Leimkühler, and A. Z. Nagel, Z. Anorg. Allg. Chem. **582**, 131 (1990).
9. J. Ravez, G. Peraudeau, H. Arend, S. C. Abrahams, and P. Hagenmuller, Ferroelectrics **26**, 767 (1980).
10. G. Peraudeau, J. Ravez, P. Hagenmüller, and H. Arend, Solid State Cummun. **27**, 591 (1978).
11. I. N. Flerov, V. D. Fokina, A. F. Bovina, E. V. Bogdanov, M. S. Molokeev, A. G. Kocharova, E. I. Pogoreltsev, and N. M. Laptash, Phys. Solid State. **50** (3), 515 (2008).
12. I. N. Flerov, M. V. Gorev, A. Tressaud, and N. M. Laptash, Crystallogr. Rep. **56** (1), 9 (2011).
13. A. K. Zvezdin and A. P. Pyatakov, Phys.—Usp. **47** (4), 416 (2004).
14. J. F. Scott and R. Blinc, J. Phys.: Condens. Matter **23**, 113202 (2011).
15. S. G. Choi, S.-J. Wang, H.-H. Park, M. P. Hong, and K.-H. Kwon, J. Vac. Sci. Technol., A **28**, 1 (2010).
16. N. Watanabe, H. Nakayama, K. Fukao, and F. Munakata, J. Appl. Phys. **110**, 023519 (2011).
17. M. V. Lobanov, A. M. Abakumov, A. V. Sidorova, M. G. Rosova, O. G. D'yachenko, E. V. Antipov, J. Hadermann, and Van G. Tendeloo, Solid State Sci. **4**, 19 (2002).
18. A. M. Alekseeva, A. M. Abakumov, M. G. Rosova, E. V. Antipov, and J. J. Hadermann, Solid State Chem. **177**, 731 (2004).
19. I. Saratovsky, M. A. Lockett, N. H. Rees, and M. A. Hayward, Inorg. Chem. **47**, 5212 (2008).
20. V. Atuchin, M. Molokeev, G. Yurkin, T. Gavrilova, V. Kesler, N. Laptash, I. Flerov, and G. Patrin, J. Phys. Chem. C **116**, 10162 (2012).
21. *Bruker AXS TOPAS V4: General Profile and Structure Analysis Software for Powder Difftaction Data: User's Manual* (Bruker AXS, Karlsruhe, Germany, 2008).
22. M. B. Smirnov and V. Yu. Kazimirov, *LADY: Software for Lattice Dymanics Simulations* (JINR Communications, Dubna, 2001), E14-2001-159.
23. M. Born and Kun Huang, *Dynamical Theory of Crystal Lattices* (Clarendon, Oxford, 1954; Inostrannaya Literatura, Moscow, 1958).
24. A. V. Kartashev, I. N. Flerov, N. V. Volkov, and K. A. Sablina, J. Magn. Magn. Mater. **322**, 622 (2010).
25. V. G. Vaks, *Introduction to the Microscopic Theory of Ferroelectrics* (Nauka, Moscow, 1973) [in Russian].
26. V. D. Fokina, I. N. Flerov, M. V. Gorev, M. S. Molokeev, A. D. Vasiliev, and N. M. Laptash, Ferroelectrics **347**, 60 (2007).

Translated by O. Borovik-Romanova